

Status of B physics CP violation. BELLE II expectations.

Indrayudh Das  
Durba Ghosh

Indian Institute of Science  
Center for High Energy Physics  
Bengaluru, India

*Review as part of the course Standard Model*

## Acknowledgements

This paper was written as part of the coursework for the course *Standard Model*. We would like to sincerely thank our instructor, Professor B. Ananthanarayan, for providing us with valuable resources and outlining the overall topics that served as a starting point for this work.

We would also like to extend our special thanks to Professor Meenakshi for her insightful explanations and clarifications on several concepts that were integral to the development of this paper.

## Abstract

The Standard Model (SM) incorporates CP violation through the irreducible complex phase in the Cabibbo-Kobayashi-Maskawa (CKM) matrix, emerging from Yukawa interactions after electroweak symmetry breaking. Diagonalization of non-diagonal mass matrices introduces flavor mixing governed by the CKM matrix, with CP violation quantified by the Jarlskog invariant  $J \approx A^2 \lambda^6 \eta$ . Three mechanisms generate observable CP violation: **(1)** direct asymmetries in decays requiring interfering amplitudes with distinct weak ( $\Delta\phi$ ) and strong ( $\Delta\delta$ ) phases, **(2)**  $|q/p| \neq 1$  in neutral meson mixing, and **(3)** interference between mixing and decay processes.

Key experimental constraints include:

- $\sin 2\beta = 0.691 \pm 0.017$  from  $B^0 \rightarrow J/\psi K_S$
- $\gamma = (65.4 \pm 1.1)^\circ$  from  $B^\pm \rightarrow D K^\pm$
- $\Delta m_{d,s}$  measurements constraining  $|V_{td}|/|V_{ts}|$

Modern experiments (Belle II:  $\mathcal{L} = 50 \text{ ab}^{-1}$ , LHCb:  $\sqrt{s} = 13 \text{ TeV}$ ) resolve  $130 \mu\text{m}$  vertex displacements, probing CKM parameters with  $< 1$

# Contents

<b>1</b>	<b>Introduction</b>	<b>6</b>
<b>2</b>	<b>Theoretical Framework: From Lagrangian to CP Violation</b>	<b>7</b>
2.1	Gauge and Fermion Sectors in the Flavor Basis . . . . .	7
2.2	Higgs Sector and Electroweak Symmetry Breaking . . . . .	8
2.3	Yukawa Interactions and Fermion Mass Generation . . . . .	9
2.4	From Flavor Basis to Mass Basis: Diagonalization and the CKM Matrix	10
2.5	Parametrization of the CKM Matrix and the Wolfenstein Expansion . .	10
2.6	General Framework: CP Transformation of Decay Amplitudes . . . .	11
2.7	Derivation of the CP Asymmetry . . . . .	12
2.8	CP Transformation and the CKM Matrix . . . . .	13
2.9	The Jarlskog Invariant . . . . .	14
2.10	Categories of CP Violation in the Standard Model . . . . .	15
<b>3</b>	<b>Meson Mixing</b>	<b>16</b>
3.1	Different ways of measuring the CP violation . . . . .	17
<b>4</b>	<b>CP Violation in B Sector</b>	<b>18</b>
4.1	CPV in the Decay . . . . .	18
4.2	Mixing-Induced (Indirect) CP Violation . . . . .	18
4.3	Time Dependent CP Asymmetry . . . . .	19
<b>5</b>	<b>Constraints on Unitarity Triangle</b>	<b>19</b>
<b>6</b>	<b>Measuring CKM Phase <math>\gamma</math></b>	<b>21</b>
<b>7</b>	<b>Measuring the Angle <math>\beta</math></b>	<b>21</b>
<b>8</b>	<b>Measuring Sides of Unitarity Triangle</b>	<b>23</b>

<b>9 Experimental Landscape</b>	<b>24</b>
9.1 Overview of key experiments: Belle II,Babar, LHCb . . . . .	24
9.2 Complementary roles of Belle II and LHCb . . . . .	24
9.3 Belle II Experiment . . . . .	24
9.3.1 KEKB . . . . .	24
9.3.2 SuperKEKB . . . . .	25
9.3.3 Belle II Detector . . . . .	25
9.4 LHCb Experiment . . . . .	31
<b>10 Experimental Results</b>	<b>32</b>
<b>11 Determination of <math> V_{ub} </math></b>	<b>35</b>
11.1 Exclusive Determination: $B \rightarrow \pi \ell \nu$ . . . . .	35
11.2 Inclusive Determination: $B \rightarrow X_u \ell \nu$ . . . . .	37
11.3 Comparison and Numerical Extraction of $ V_{ub} $ . . . . .	38
<b>12 Conclusion</b>	<b>39</b>

# 1 Introduction

The violation of charge-parity (CP) symmetry stands as one of the most consequential phenomena in particle physics, essential for explaining the matter-antimatter asymmetry of the universe. Within the Standard Model (SM), CP violation arises exclusively from the irreducible complex phase in the Cabibbo-Kobayashi-Maskawa (CKM) matrix **Kobayashi 1973**, which governs flavor transitions in weak interactions. While the CKM mechanism successfully accounts for observed CP-violating effects, its minimal implementation—with a single Jarlskog invariant  $J \approx (3.0 \pm 0.2) \times 10^{-5}$ —leaves unresolved fundamental questions about the SM’s sufficiency to explain the cosmological baryon asymmetry.

This work synthesizes the theoretical and experimental foundations of CP violation in the quark sector, focusing on three interconnected themes:

1. **Mechanism:** How electroweak symmetry breaking and Yukawa interactions generate the CKM matrix, with its phase structure encoded in the Wolfenstein parameters  $(\lambda, A, \bar{\rho}, \bar{\eta})$ ;
2. **Observables:** The classification of CP violation into direct, indirect, and mixing-decay interference effects, quantified through asymmetries in  $B$ -meson decays;
3. **Tests:** Precision determinations of CKM parameters using modern experiments (Belle II, LHCb) and persistent tensions between inclusive/exclusive methods.

Recent advances in flavor physics have sharpened these tests to unprecedented precision. Time-dependent CP asymmetry measurements in  $B^0 \rightarrow J/\psi K_S$  constrain  $\sin 2\beta$  to  $\pm 0.017$  **BaBar2013**, while interference in  $B^\pm \rightarrow D K^\pm$  decays pins  $\gamma$  to  $(65.4 \pm 1.1)^\circ$  **LHCb2022**. Yet discrepancies persist, most notably the  $2.5\sigma$  tension between inclusive ( $|V_{ub}| = 4.13(25) \times 10^{-3}$ ) and lattice QCD-based exclusive determinations **FLAG2023**. These anomalies motivate both theoretical refinements in non-perturbative QCD and experimental upgrades to Belle II ( $50 \text{ ab}^{-1}$ ) and LHCb’s Run 3.

## 2 Theoretical Framework: From Lagrangian to CP Violation

The Standard Model (SM) is a gauge theory based on the symmetry group

$$G_{\text{SM}} = SU(3)_C \times SU(2)_L \times U(1)_Y.$$

Its full Lagrangian can be split into four main sectors:

$$\mathcal{L}_{\text{SM}} = \underbrace{\mathcal{L}_{\text{gauge}}}_{\text{Gauge Sector}} + \underbrace{\mathcal{L}_{\text{fermion}}}_{\text{Fermion Sector}} + \underbrace{\mathcal{L}_{\text{Higgs}}}_{\text{Higgs Sector}} + \underbrace{\mathcal{L}_{\text{Yukawa}}}_{\text{Yukawa Sector}}.$$

In what follows we present a rigorous derivation starting from the flavor basis Lagrangian, describe electroweak symmetry breaking via the Higgs mechanism, detail the fermion mass generation and the transition to the mass basis, and finally discuss the resulting charged current interactions, the CKM matrix, its Wolfenstein parametrization, and the origin of CP violation.

### 2.1 Gauge and Fermion Sectors in the Flavor Basis

In the SM before spontaneous symmetry breaking the fermions are arranged according to their weak interactions. For quarks the left-handed fields are grouped into weak doublets

$$Q_{iL} = \begin{pmatrix} u_{iL} \\ d_{iL} \end{pmatrix}, \quad (i = 1, 2, 3),$$

and the right-handed fields are singlets:

$$u_{iR}, \quad d_{iR}.$$

The fermion kinetic term, incorporating interactions with gauge fields through the covariant derivative, is written as

$$\mathcal{L}_{\text{fermion}} = \sum_{i=1}^3 \bar{Q}_{iL} i\gamma^\mu D_\mu Q_{iL} + \sum_{i=1}^3 [\bar{u}_{iR} i\gamma^\mu D_\mu u_{iR} + \bar{d}_{iR} i\gamma^\mu D_\mu d_{iR}],$$

with the covariant derivative defined by

$$D_\mu = \partial_\mu + ig_s G_\mu^a T^a + ig W_\mu^i \tau^i + ig' B_\mu Y.$$

The gauge sector itself is described by the field strength tensors:

$$G_{\mu\nu}^a = \partial_\mu G_\nu^a - \partial_\nu G_\mu^a + g_s f^{abc} G_\mu^b G_\nu^c, \quad a = 1, \dots, 8, \quad (1)$$

$$W_{\mu\nu}^i = \partial_\mu W_\nu^i - \partial_\nu W_\mu^i + g \epsilon^{ijk} W_\mu^j W_\nu^k, \quad i = 1, 2, 3, \quad (2)$$

$$B_{\mu\nu} = \partial_\mu B_\nu - \partial_\nu B_\mu. \quad (3)$$

Thus, the gauge kinetic Lagrangian is

$$\mathcal{L}_{\text{gauge}} = -\frac{1}{4} G_{\mu\nu}^a G^{a\mu\nu} - \frac{1}{4} W_{\mu\nu}^i W^{i\mu\nu} - \frac{1}{4} B_{\mu\nu} B^{\mu\nu}.$$

In the flavor basis, the charged current interactions mediated by the  $W^\pm$  bosons appear as

$$\mathcal{L}_{\text{CC}} = -\frac{g}{\sqrt{2}} \sum_{i=1}^3 \bar{u}_{iL} \gamma^\mu d_{iL} W_\mu^+ + \text{h.c.},$$

where the up-type and down-type quarks are not yet the physical mass eigenstates.

## 2.2 Higgs Sector and Electroweak Symmetry Breaking

To give masses to the gauge bosons and fermions, the Higgs mechanism introduces a complex scalar doublet

$$\Phi = \begin{pmatrix} \phi^+ \\ \phi^0 \end{pmatrix}, \quad Y(\Phi) = \frac{1}{2}.$$

The Higgs Lagrangian is written as

$$\mathcal{L}_{\text{Higgs}} = (D_\mu \Phi)^\dagger (D^\mu \Phi) - V(\Phi),$$

with potential

$$V(\Phi) = \mu^2 \Phi^\dagger \Phi + \lambda (\Phi^\dagger \Phi)^2.$$

For  $\mu^2 < 0$  the potential minimizes for nonzero field values. The vacuum expectation value (vev) of the neutral component is chosen as

$$\langle \Phi \rangle = \frac{1}{\sqrt{2}} \begin{pmatrix} 0 \\ v \end{pmatrix}, \quad \text{with } v = \sqrt{-\mu^2/\lambda} \approx 246 \text{ GeV}.$$

In the unitary gauge we write

$$\Phi(x) = \frac{1}{\sqrt{2}} \begin{pmatrix} 0 \\ v + h(x) \end{pmatrix},$$

where  $h(x)$  is the physical Higgs boson. The covariant derivative acting on  $\Phi$  is

$$D_\mu \Phi = \left( \partial_\mu + i\frac{g}{2}\tau^i W_\mu^i + i\frac{g'}{2}B_\mu \right) \Phi.$$

Expanding  $|D_\mu \Phi|^2$  results in mass terms for the  $W$  and  $Z$  bosons:

$$M_W = \frac{1}{2}gv, \quad M_Z = \frac{1}{2}\sqrt{g^2 + g'^2} v,$$

while the photon remains massless. The photon field  $A_\mu$  is defined via the Weinberg angle  $\theta_W$  by

$$A_\mu = \sin \theta_W W_\mu^3 + \cos \theta_W B_\mu, \quad \sin \theta_W = \frac{g'}{\sqrt{g^2 + g'^2}}.$$

### 2.3 Yukawa Interactions and Fermion Mass Generation

Fermion masses are generated by Yukawa interactions between the fermions and the Higgs field. For the quark sector, the Yukawa Lagrangian is

$$\mathcal{L}_{\text{Yukawa}} = - \sum_{i,j=1}^3 \left[ \bar{Q}_{iL} Y_{ij}^d \Phi d_{jR} + \bar{Q}_{iL} Y_{ij}^u \tilde{\Phi} u_{jR} \right] + \text{h.c.},$$

with

$$\tilde{\Phi} = i\tau_2 \Phi^* = \begin{pmatrix} \phi^{0*} \\ -\phi^- \end{pmatrix}.$$

After spontaneous symmetry breaking where  $\Phi \rightarrow \frac{1}{\sqrt{2}} \begin{pmatrix} 0 \\ v \end{pmatrix}$ , the Yukawa Lagrangian yields mass terms:

$$\mathcal{L}_{\text{Yukawa}} \supset -\frac{v}{\sqrt{2}} \sum_{i,j=1}^3 \left[ \bar{d}_{iL} Y_{ij}^d d_{jR} + \bar{u}_{iL} Y_{ij}^u u_{jR} \right] + \text{h.c.}.$$

Thus, the quark mass matrices are identified as

$$(M_d)_{ij} = \frac{v}{\sqrt{2}} Y_{ij}^d, \quad (M_u)_{ij} = \frac{v}{\sqrt{2}} Y_{ij}^u.$$

## 2.4 From Flavor Basis to Mass Basis: Diagonalization and the CKM Matrix

In general, the mass matrices  $M_u$  and  $M_d$  are complex and not diagonal in the flavor basis. They are diagonalized by unitary transformations:

$$u_L = U_{u,L} u_L^{(\text{mass})}, \quad u_R = U_{u,R} u_R^{(\text{mass})},$$

$$d_L = U_{d,L} d_L^{(\text{mass})}, \quad d_R = U_{d,R} d_R^{(\text{mass})},$$

so that

$$U_{u,L}^\dagger M_u U_{u,R} = M_u^{\text{diag}}, \quad U_{d,L}^\dagger M_d U_{d,R} = M_d^{\text{diag}}.$$

While the Yukawa interactions were originally given in the flavor basis, the physical phenomena (mass spectra, decay rates, etc.) are governed by the mass basis. In particular, the charged current Lagrangian in the flavor basis,

$$\mathcal{L}_{\text{CC}} = -\frac{g}{\sqrt{2}} \bar{u}_L \gamma^\mu d_L W_\mu^+ + \text{h.c.},$$

transforms to the mass basis via the unitary rotations:

$$\bar{u}_L \gamma^\mu d_L = \bar{u}_L^{(\text{mass})} (U_{u,L}^\dagger U_{d,L}) \gamma^\mu d_L^{(\text{mass})}.$$

The combination

$$V \equiv U_{u,L}^\dagger U_{d,L},$$

is the Cabibbo–Kobayashi–Maskawa (CKM) matrix. In the mass basis the charged current Lagrangian becomes

$$\mathcal{L}_{\text{CC}} = -\frac{g}{\sqrt{2}} \bar{u}_L^{(\text{mass})} \gamma^\mu V d_L^{(\text{mass})} W_\mu^+ + \text{h.c.}.$$

The unitary CKM matrix encapsulates the flavor mixing among different quark generations and is the sole source of CP violation in the quark sector of the SM.

## 2.5 Parametrization of the CKM Matrix and the Wolfenstein Expansion

Being a  $3 \times 3$  unitary matrix, the CKM matrix has nine real parameters; however, by appropriately redefining the quark phases, only four physical parameters remain. One

common parametrization is to write the CKM matrix in a factorized form in terms of three Euler rotation angles  $\theta_{12}$ ,  $\theta_{13}$ ,  $\theta_{23}$  and one CP-violating phase  $\delta$ . A typical factorized parametrization is

$$V = \begin{pmatrix} 1 & 0 & 0 \\ 0 & c_{23} & s_{23} \\ 0 & -s_{23} & c_{23} \end{pmatrix} \begin{pmatrix} c_{13} & 0 & s_{13}e^{-i\delta} \\ 0 & 1 & 0 \\ -s_{13}e^{i\delta} & 0 & c_{13} \end{pmatrix} \begin{pmatrix} c_{12} & s_{12} & 0 \\ -s_{12} & c_{12} & 0 \\ 0 & 0 & 1 \end{pmatrix}, \quad (4)$$

with  $c_{ij} = \cos \theta_{ij}$  and  $s_{ij} = \sin \theta_{ij}$ . Multiplying out these matrices yields the standard form

$$V = \begin{pmatrix} c_{12}c_{13} & s_{12}c_{13} & s_{13}e^{-i\delta} \\ -c_{12}s_{23}s_{13}e^{i\delta} - s_{12}c_{23} & -s_{12}s_{23}s_{13}e^{i\delta} + c_{12}c_{23} & s_{23}c_{13} \\ s_{12}s_{23} - c_{12}c_{23}s_{13}e^{i\delta} & -c_{12}s_{23} - s_{12}c_{23}s_{13}e^{i\delta} & c_{23}c_{13} \end{pmatrix}. \quad (5)$$

For many physical applications the mixing angles are small (especially  $\theta_{13}$  and  $\theta_{23}$ ); therefore, it is useful to employ the Wolfenstein parametrization. In this expansion one defines

$$\lambda \equiv s_{12} \approx 0.22,$$

and introduces the parameters  $A$ ,  $\rho$ , and  $\eta$  such that the CKM matrix reads

$$V \approx \begin{pmatrix} 1 - \frac{\lambda^2}{2} & \lambda & A\lambda^3(\rho - i\eta) \\ -\lambda & 1 - \frac{\lambda^2}{2} & A\lambda^2 \\ A\lambda^3(1 - \rho - i\eta) & -A\lambda^2 & 1 \end{pmatrix} + \mathcal{O}(\lambda^4). \quad (6)$$

The parameter  $\eta$  is directly responsible for CP-violating effects. Although this expansion is approximate—unitarity is not exact at finite order—it is an excellent representation due to the smallness of  $\lambda$  and the higher-order corrections.

## 2.6 General Framework: CP Transformation of Decay Amplitudes

In the Standard Model the only source of CP violation in the quark sector is the nonzero complex phase in the Cabibbo–Kobayashi–Maskawa (CKM) matrix. In this section, we rigorously show how a complex phase results in CP-violating observables.

Consider a generic decay of a meson  $B$  to a final state  $f$ . Suppose that the amplitude for the decay can be written as a sum of (at least) two interfering contributions:

$$A_f = A_1 e^{i\delta_1} e^{i\phi_1} + A_2 e^{i\delta_2} e^{i\phi_2}, \quad (7)$$

where:

- $A_i$  are real and positive amplitudes,
- $\delta_i$  are the strong (CP-even) phases arising from final-state interactions,
- $\phi_i$  are the weak (CP-odd) phases arising from the complex elements of the CKM matrix.

Under the CP transformation, the weak phases reverse sign while the strong phases (arising from QCD interactions, assumed to be CP invariant) remain unchanged. Consequently, the CP-conjugate decay amplitude is given by

$$\bar{A}_{\bar{f}} = A_1 e^{i\delta_1} e^{-i\phi_1} + A_2 e^{i\delta_2} e^{-i\phi_2}. \quad (8)$$

A measure of direct CP violation in the decay is the asymmetry

$$A_{CP} = \frac{|A_f|^2 - |\bar{A}_{\bar{f}}|^2}{|A_f|^2 + |\bar{A}_{\bar{f}}|^2}. \quad (9)$$

Let us now see explicitly that a non-vanishing  $\phi_i$  (with a relative weak phase) leads to  $A_{CP} \neq 0$ .

## 2.7 Derivation of the CP Asymmetry

First, write the squared modulus of the amplitude in Eq. (7):

$$\begin{aligned} |A_f|^2 &= \left| A_1 e^{i\delta_1} e^{i\phi_1} + A_2 e^{i\delta_2} e^{i\phi_2} \right|^2 \\ &= A_1^2 + A_2^2 + 2 A_1 A_2 \cos [(\delta_2 - \delta_1) + (\phi_2 - \phi_1)]. \end{aligned} \quad (10)$$

Similarly, for the CP-conjugate process in Eq. (8) we obtain:

$$\begin{aligned} |\bar{A}_{\bar{f}}|^2 &= |A_1 e^{i\delta_1} e^{-i\phi_1} + A_2 e^{i\delta_2} e^{-i\phi_2}|^2 \\ &= A_1^2 + A_2^2 + 2 A_1 A_2 \cos [(\delta_2 - \delta_1) - (\phi_2 - \phi_1)]. \end{aligned} \quad (11)$$

Subtracting Eq. (11) from Eq. (10) gives:

$$\begin{aligned} |A_f|^2 - |\bar{A}_{\bar{f}}|^2 &= 2 A_1 A_2 \left\{ \cos [(\delta_2 - \delta_1) + (\phi_2 - \phi_1)] - \cos [(\delta_2 - \delta_1) - (\phi_2 - \phi_1)] \right\} \\ &= -4 A_1 A_2 \sin(\delta_2 - \delta_1) \sin(\phi_2 - \phi_1). \end{aligned} \quad (12)$$

Thus, the CP asymmetry defined in Eq. (9) becomes (to leading order)

$$A_{CP} = -\frac{4 A_1 A_2 \sin(\delta_2 - \delta_1) \sin(\phi_2 - \phi_1)}{2(A_1^2 + A_2^2) + 4 A_1 A_2 \cos(\delta_2 - \delta_1) \cos(\phi_2 - \phi_1)}. \quad (13)$$

It is clear from this expression that if either the weak phase difference  $\phi_2 - \phi_1$  or the strong phase difference  $\delta_2 - \delta_1$  vanishes, then  $A_{CP} = 0$ . In our context the weak phases are determined by the complex entries of the CKM matrix. Therefore, a nonzero  $\phi_2 - \phi_1$  signals CP violation.

## 2.8 CP Transformation and the CKM Matrix

In the quark sector the charged current interaction in the mass basis is given by

$$\mathcal{L}_{CC} = -\frac{g}{\sqrt{2}} \bar{u}_L^{(\text{mass})} \gamma^\mu V d_L^{(\text{mass})} W_\mu^+ + \text{h.c.}, \quad (14)$$

with  $V$  the CKM matrix. Under a CP transformation the quark fields transform as

$$u_L^{(\text{mass})}(x) \xrightarrow{CP} \eta_u \gamma^0 (u_L^{(\text{mass})})^*(\tilde{x}), \quad d_L^{(\text{mass})}(x) \xrightarrow{CP} \eta_d \gamma^0 (d_L^{(\text{mass})})^*(\tilde{x}), \quad (15)$$

where  $\tilde{x} = (t, -\mathbf{x})$  and  $\eta_u, \eta_d$  are arbitrary phase factors that can be chosen appropriately. Under CP the  $W$  field transforms as

$$W_\mu^+(x) \xrightarrow{CP} -W^{-\mu}(\tilde{x}). \quad (16)$$

Assuming the strong and electromagnetic interactions conserve CP, one may show that the only possible source of CP violation in  $\mathcal{L}_{\text{CC}}$  is from the complex phases of the CKM matrix. In fact, under CP the charged current Lagrangian becomes

$$\begin{aligned} \mathcal{L}_{\text{CC}}(x) &\xrightarrow{\text{CP}} -\frac{g}{\sqrt{2}}\eta_u^*\eta_d \bar{u}_L^{(\text{mass})}(\tilde{x}) \gamma^\mu V^* d_L^{(\text{mass})}(\tilde{x}) W^-_\mu(\tilde{x}) + \text{h.c.} \\ &\neq \mathcal{L}_{\text{CC}}(\tilde{x}), \end{aligned} \quad (17)$$

unless the CKM matrix is real (i.e.  $V = V^*$  modulo rephasing, which is not possible in the presence of a non-vanishing physical phase). Thus, the transformation of the CKM matrix is

$$V \xrightarrow{\text{CP}} V^*. \quad (18)$$

If  $V$  were real then  $V^* = V$  and no CP violation would arise from the charged current interactions. The fact that experiments measure CP-violating observables implies that the CKM matrix contains irreducible complex phases.

## 2.9 The Jarlskog Invariant

A rephasing-invariant measure of CP violation is provided by the Jarlskog invariant  $J$ , defined as

$$J = \Im[V_{ij} V_{kl} V_{il}^* V_{kj}^*], \quad (19)$$

where the indices  $i$ ,  $j$ ,  $k$ , and  $l$  are all different. The important property of  $J$  is that it is independent of the phase redefinitions of the quark fields. A necessary and sufficient condition for CP conservation in the Standard Model is

$$J = 0.$$

A nonzero value of  $J$  is therefore a rigorous indicator of CP violation. When the CKM matrix is parameterized in the standard form (or the Wolfenstein form),  $J$  is approximately given by

$$J \approx A^2 \lambda^6 \eta, \quad (20)$$

where  $\lambda$ ,  $A$ , and  $\eta$  are the Wolfenstein parameters. The numerical smallness of  $\lambda \approx 0.22$  and the size of  $J$  explain why CP-violating effects are small in the quark sector.

## 2.10 Categories of CP Violation in the Standard Model

There are three main categories where CP violation manifests:

1. **Direct CP Violation:** In decays where the amplitude can be written as a sum of two interfering parts,

$$A_f = A_1 e^{i\delta_1} e^{i\phi_1} + A_2 e^{i\delta_2} e^{i\phi_2},$$

the CP-conjugate process has amplitude

$$\overline{A}_f = A_1 e^{i\delta_1} e^{-i\phi_1} + A_2 e^{i\delta_2} e^{-i\phi_2}.$$

The CP asymmetry,

$$A_{CP} = \frac{|A_f|^2 - |\overline{A}_f|^2}{|A_f|^2 + |\overline{A}_f|^2},$$

is non-zero provided that there is a non-vanishing weak phase difference ( $\phi_2 - \phi_1$ ) and a nonzero strong phase difference ( $\delta_2 - \delta_1$ ).

2. **Indirect CP Violation in Mixing:** For neutral meson systems (e.g.,  $B^0 - \overline{B^0}$ ), mixing occurs via one-loop box diagrams and the physical mass eigenstates are mixtures of the flavor eigenstates:

$$B_{L,H} = p B^0 \pm q \overline{B^0}.$$

If CP were conserved in mixing,  $|q/p| = 1$ ; deviations indicate CP violation in the mixing dynamics.

3. **CP Violation in the Interference between Mixing and Decay:** In decays to a common CP eigenstate  $f_{CP}$ , the time-dependent decay rate is given by

$$\Gamma(B^0(t) \rightarrow f_{CP}) \propto e^{-\Gamma t} \left[ 1 + S_{CP} \sin(\Delta m t) - C_{CP} \cos(\Delta m t) \right],$$

where  $S_{CP}$  and  $C_{CP}$  are sensitive to the interference between direct decays and those following mixing. For example, in  $B^0 \rightarrow J/\psi K_S$  one obtains

$$S_{J/\psi K_S} = \sin 2\beta,$$

with  $\beta$  directly related to the CKM elements.

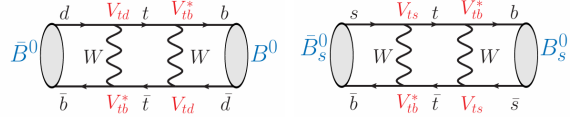


Figure 1: The SM diagrams leading to  $B_d$  (left) and  $B_s$  mixing (right).

### 3 Meson Mixing

The term mixing denotes that the flavour eigenstates do not equal mass eigenstates, i.e., that the eigenstates of the SM Hamiltonian are composed of states with different flavour compositions.

$B^0 \sim \bar{b}d$  and  $\bar{B}^0 \sim b\bar{d}$  are flavour eigenstates but are not mass eigenstates. The mass eigenstates are admixtures of them. The term oscillations denotes that the initial flavour eigenstate time evolves to a different flavour eigenstate. The reason for this is that the flavour eigenstates are composed from two mass eigenstates, each of which evolves slightly differently.

The oscillation frequency is the energy splitting,  $\omega = \Delta E$ .

In rest frame  $\Delta E = \Delta m$ .

But  $B^+(\bar{b}u)$  and  $B^-(b\bar{u})$  do not mix.  $U(1)_{em}$  gauge symmetry forbids such mixings.

$B^0(\bar{b}d)$  and  $\bar{B}^0(b\bar{d})$  mixes. But such FCNCs are forbidden in tree-level but are allowed at 1 loop level.

If CP is conserved, the mass eigenstates are

$$|B_{L,H}\rangle = (|B^0\rangle \pm |\bar{B}^0\rangle) \frac{1}{\sqrt{2}} \quad (21)$$

$$CP|B_{L,H}\rangle = \pm |B_{L,H}\rangle \quad (22)$$

If CP is violated then mass eigenstates are

$$|B\rangle_{L,H} = p|B^0\rangle \pm q|\bar{B}^0\rangle \quad (23)$$

where  $p=q=\frac{1}{\sqrt{2}}$  if CP is conserved.

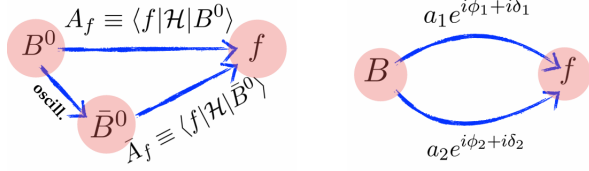


Figure 2: Left: The two different paths for a  $B^0$  meson to decay to a final state  $f$ . Right: two interfering amplitudes are required to have direct CPV.

### 3.1 Different ways of measuring the CP violation

CP violation is an inherently quantum mechanical effect. In order to be sensitive to a phase an interference is needed. Thus, CP violating observables necessarily require some kind of interference. Depending on the type of interference there are three distinct categories of CP violating observables

- **CPV in the Decay** It is also called direct CPV, occurs when there is interference between different contributions to the decay amplitudes so that

$$|A_f| \neq |\overline{A}_f| \quad (24)$$

where

$$A_f = \langle f | H | B^0 \rangle \quad (25)$$

$$\overline{A}_f = \langle f | H | \overline{B}^0 \rangle \quad (26)$$

- **CPV in Mixing** This arises when  $|q/p| \neq 1$ , and corresponds to interference between different ways to oscillate between  $B^0$  and  $\overline{B}^0$  states.
- **CPV in Interference** Interference between decays with and without mixing, arises when  $Im\lambda_f \neq 0$  where

$$\lambda_f = \frac{q\bar{A}_f}{pA_f}. \quad (27)$$

Here the interference is between two different paths of  $B^0$  to decay to the final states  $f$ , see Fig. 2. The two paths are either through direct decay, proportional to  $A_f$ , or by first oscillating to  $B^0$ , which then decays to  $f$ , giving a contribution proportional to  $(q/p)A_f$ .

## 4 CP Violation in B Sector

### 4.1 CPV in the Decay

The CPV observable is the decay asymmetry

$$A_f = \frac{\Gamma(\bar{B} \rightarrow \bar{f}) - \Gamma(B \rightarrow f)}{\Gamma(\bar{B} \rightarrow \bar{f}) + \Gamma(B \rightarrow f)} \quad (28)$$

This occurs when the decay amplitudes of a particle and its CP-conjugate process have different magnitudes or phases. Suppose a decay amplitude can be written as a sum of two interfering contributions:

$$A = A_1 e^{i\delta_1} e^{i\phi_1} + A_2 e^{i\delta_2} e^{i\phi_2}, \quad (29)$$

where  $A_i$  are the magnitudes,  $\delta_i$  are the strong (CP-even) phases from QCD interactions, and  $\phi_i$  are the weak (CP-odd) phases from the CKM matrix. The CP-conjugate amplitude is

$$\bar{A} = A_1 e^{i\delta_1} e^{-i\phi_1} + A_2 e^{i\delta_2} e^{-i\phi_2}. \quad (30)$$

The CP asymmetry is then defined as:

$$A_{CP} = \frac{|A|^2 - |\bar{A}|^2}{|A|^2 + |\bar{A}|^2}. \quad (31)$$

$$A_{CP} = \frac{A_2}{A_1} \sin(\phi_2 - \phi_1) \sin(\delta_2 - \delta_1) \quad (32)$$

Non-zero  $A_{CP}$  requires non zero contribution in both the amplitudes and both a difference in weak phases ( $\phi_1 \neq \phi_2$ ) and a non-zero difference in strong phases ( $\delta_1 \neq \delta_2$ ). This type of CP violation is directly observable in decay rates.

### 4.2 Mixing-Induced (Indirect) CP Violation

Mixing-induced CP violation arises from the interference between decays with and without mixing. For neutral B mesons, which can oscillate between  $B^0$  and  $\bar{B}^0$ .

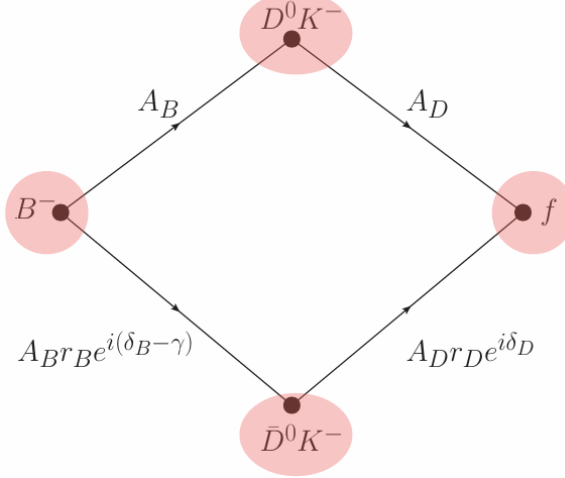


Figure 3: The two interfering amplitudes.

### 4.3 Time Dependent CP Asymmetry

Time-dependent decay rates into a common CP eigenstate  $f_{CP}$  can be written as

$$\Gamma(B^0(t) \rightarrow f_{CP}) \propto e^{-\Gamma t} [1 + S_{CP} \sin(\Delta m t) - C_{CP} \cos(\Delta m t)], \quad (33)$$

and

$$A_{CP}(t) = S_{CP} \sin \Delta m t - C_{CP} \cos \Delta m t \quad (34)$$

where

- $C_{CP}$  measures direct CP violation in the decay,
- $S_{CP}$  measures mixing-induced CP violation and is related to the interference between decays with and without mixing.

## 5 Constraints on Unitarity Triangle

- **Yellow Circle** It is constraint by  $\Delta m_d$  (mass difference between of the mass eigenstates made of  $B^0$  and  $\bar{B}^0$ .  $\Delta m_d$  is measured from the time dependent oscillations in  $B^0 \rightarrow J/\psi K_s$ .

$$\Delta m_d \propto |V_{td}|^2 \quad (35)$$

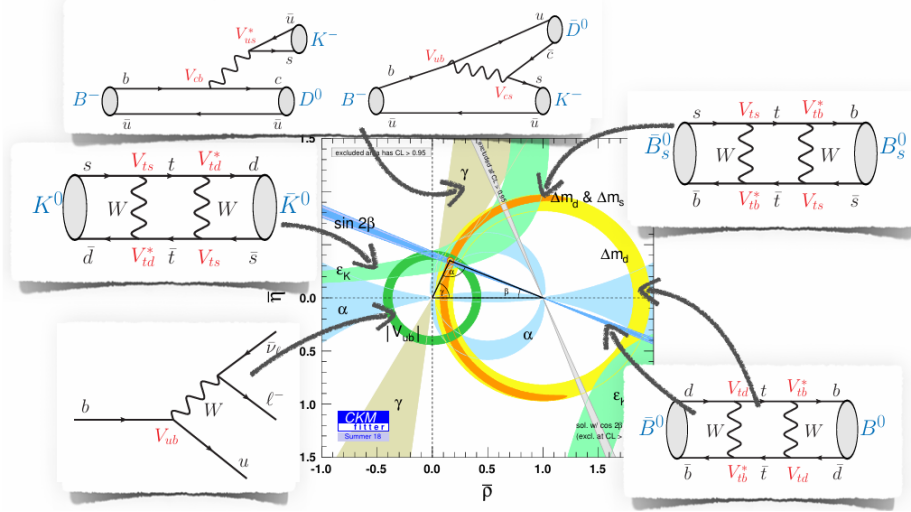


Figure 4: Some of the main CKM constraints and the respective SM diagrams.

$$V_{td} = A\lambda^3(1 - \bar{\rho} - i\bar{\eta}) \quad (36)$$

$$|V_{td}|^2 = A^2\lambda^6[(1 - \bar{\rho})^2 + \bar{\eta}^2] \quad (37)$$

$$(1 - \bar{\rho})^2 + \bar{\eta}^2 = \frac{\Delta m_d}{A^2\lambda^6} \quad (38)$$

which is a equation of a circle centred at  $(1,0)$  and radius  $\propto \sqrt{\Delta m_d}$ .

- **Orange Half Circle** It is constraint by  $\Delta m_s$  (mass difference between the mass eigenstates made of  $B_s^0$  and  $\bar{B}_s^0$ ). It actually constrains the ratio  $\frac{V_{td}}{V_{ts}}$  which defines a circle in complex plane.
- **Blue Band** It comes from CP violation in the decay  $B^0 \rightarrow J/\psi K_s$ . It gives the  $\beta$  angle and fixes the orientation.
- **Green Hyperbola** It is constraint by  $\epsilon_k$ . It measures indirect CP violation in the neutral K Meson system (mixing between  $K^0$  and  $\bar{K}^0$ ).
- **Brown Wedge** It gives us  $\gamma$  angle which is the phase of  $V_{ub}$ . It is measured from the CP asymmetry in  $B^+ \rightarrow DK^+$ .

$$\gamma = \tan^{-1}\left(\frac{\bar{\eta}}{\bar{\rho}}\right) = \arg(V_{ub}^*) \quad (39)$$

- **Green circle** It determines the length of one side of the triangle. It is constraint by  $\frac{|V_{ub}|}{|V_{cb}|}$ . It comes from semileptonic decays  $B \rightarrow \Pi l \nu$  and  $B \rightarrow D l \nu$ .
- **Blue Wedge** It gives us the angle  $\alpha$ . It comes from  $B^0 \rightarrow \pi^+ \pi^-$ .

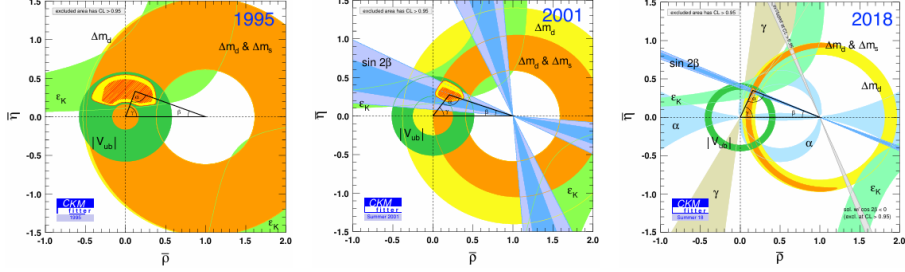


Figure 5: The evolution of the constraints in the standard CKM unitarity triangle plane from 1995(left),to just after the start of B factories (middle),to the present(right).Taken from the ckm fitter website

## 6 Measuring CKM Phase $\gamma$

- The interference term in  $B^- \rightarrow [D \rightarrow f]K^-$  is proportional to  $(\delta_B + \delta_D - \gamma)$  and the interference term in  $B^+ \rightarrow [D \rightarrow \bar{f}]K^+$  is proportional to  $(\delta_B + \delta_D + \gamma)$ .
- The difference of the two thus gives the quantity we are after  $\gamma$ .
- $A_{CP} = r_B r_D \sin(\delta_B + \delta_D) \sin \gamma$ . If the hadronic parameters are known we can calculate  $\gamma$ . The experimental value is  $(65.4 \pm 1.1)^\circ$

That all the hadronic uncertainties can be obtained experimentally makes this approach a very powerful tool. It means that the angle  $\gamma$  can be extracted with basically no theory uncertainties. The theoretical corrections arise only from one loop electroweak corrections, limiting the ultimate precision with which can be extracted up to minuscule  $\gamma_{th} \lesssim 10^{-7}$ . The experimental error bars will be larger than this for a long time. At present they are at  $\delta_\gamma \lesssim 6$ .

## 7 Measuring the Angle $\beta$

The  $q/p$  does not depend on the final state  $f$ , and is the property of the  $B0 - \bar{B}0$  system. In the SM it is given by the ratio of one loop diagram and its complex conjugated version, so that

$$\frac{q}{p} = e^{-i\phi_B} = \frac{V_{tb}^* V_{td}}{V_{tb} V_{td}^*} \quad (40)$$

with hadronic matrix elements cancelling in the ratio.

- The decay  $B^0 \rightarrow J/\psi K_S^0$  is used to extract  $\beta$ . To a good approximation it is given by the ratio of the CKM elements

$$\frac{\bar{A}_{J/\psi K_s}}{A_{J/\psi K_s}} = \eta_f \frac{V_{cb} V_{cs}^*}{V_{cb}^* V_{cs}} + \dots, \quad (41)$$

Therefore

$$\lambda_{J/\psi K_s} = \eta_f \frac{V_{tb}^* V_{tb} V_{cb} V_{cs}^*}{V_{tb} V_{td}^* V_{cb}^* V_{cs}} = \eta_f e^{-2i\beta} \quad (42)$$

and thus

$$Im \lambda_{J/\psi K_s} = \sin 2\beta = 0.691 \pm 0.017 \quad (43)$$

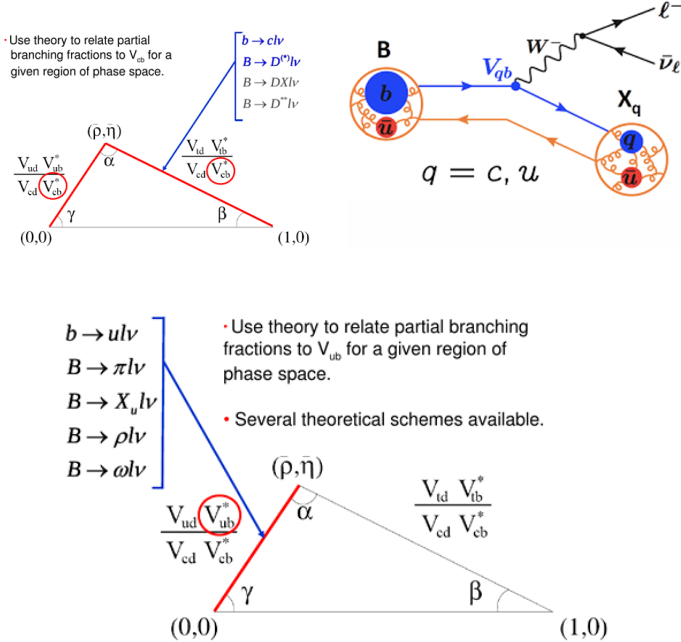
This is world average (PDG 2023) value of  $\beta$

- The time-dependent CP asymmetry is given by:

$$A_{CP}(t) = S_f \sin(\Delta m_d t) - C_f \cos(\Delta m_d t),$$

where:

$$S_f = \sin(2\beta) \quad \text{and} \quad C_f \approx 0.$$



## 8 Measuring Sides of Unitarity Triangle

- Sides are combinations of magnitudes of CKM matrix elements
- Heavy flavor decays one way to measure these.
  - $V_{cd}$  from  $D_s \rightarrow Kl\nu$ ,  $D \rightarrow \pi l\nu$ .
  - $V_{cs}$  from  $D_s^+ \rightarrow \mu^+\nu, D \rightarrow Kl\nu$ .
  - $V_{cb}$  from  $B \rightarrow X_c l\nu, (X_c: D, D^*$  etc).
  - $V_{ub}$  from  $B \rightarrow X_c l\nu, (X_d: D, D^*$  etc)

Current values:

$$|V| = \begin{pmatrix} 0.97 \pm 0.0001 & 0.22 \pm 0.001 & 0.0039 \pm 0.0004 \\ 0.23 \pm 0.01 & 1.02 \pm 0.04 & 0.0041 \pm 0.001 \\ 0.0084 \pm 0.0006 & 0.039 \pm 0.002 & 0.88 \pm 0.07 \end{pmatrix} \quad (44)$$

## 9 Experimental Landscape

### 9.1 Overview of key experiments: Belle II,Babar, LHCb

The constraints on the CKM Unitarity Triangle is coming from the  $B_0, B_d^+$  mesons from measurements at Belle , BaBar and LHCb,  $B_s$  meson and  $\lambda_b$  baryon from measurement at LHCb. The upshot of these results is that the KM mechanism is the dominant origin of CPV.

### 9.2 Complementary roles of Belle II and LHCb

Belle II operates as an electron-positron collider tuned to the  $\gamma(4S)$  resonance (around 10.58 GeV). This resonance has just enough energy to decay into a pair of  $B^+B^-$  and  $B^0\bar{B}^0$  mesons.Belle II contributes with high-precision measurements in a controlled environment.

LHCb operates in the environment of the Large Hadron Collider (LHC), where high-energy proton-proton collisions produce a wide variety of B mesons and b baryons(e.g.  $B_s, \lambda_b$ ).LHCb adds complementary information from a richer b-hadron spectrum.

### 9.3 Belle II Experiment

#### 9.3.1 KEKB

- KEKB was the asymmetric  $e^-$  (8 GeV),  $e^+$  (3.5 GeV) collider located at the High Energy Accelerator Research Organization (KEK) in Tsukuba, Japan, produces large numbers of B mesons to study CP violation.
- It is operated from 1999 to 2010 .
- KEKB collided electrons and positrons at a center-of-mass energy near the  $\Upsilon(4S)$  resonance (about 10.58 GeV), which decays into  $B^+, B^-$  pairs.
- Luminosity =  $2.11 \text{ cm}^{-2} \text{ s}^{-2}$

### 9.3.2 SuperKEKB

- After KEKB shut down in 2010, it was upgraded to SuperKEKB. It has higher luminosity. It started operating in 2018.
- It has Luminosity =  $80 \text{ cm}^{-2} \text{ s}^{-2}$  ( $40 \times$  KEKB).
- Asymmetric  $e^-$ (7 GeV),  $e^+$ (4 GeV) beam.
- It uses nano beam scheme.

Entity	KEKB	SuperKEKB
$\mathcal{L} (10^{34} \frac{1}{\text{s.cm}^2})$	2.11	80 ( $\times 40$ )
$\int \mathcal{L} dt (ab^{-1})$	0.8	50
$e^-/e^+ E(\text{GeV})$	8/3.5	7/4
$e^-/e^+ I(A)$	1.6/1.9	2.6/3.6(2)
$\beta\gamma$	0.45	0.28
$\langle \Delta z \rangle (\mu\text{m})$	$\sim 200$	$\sim 130$

### 9.3.3 Belle II Detector

- Belle II is the upgraded detector at SuperKEKB.
- Hermite Detector: Full event reconstruction.
- Excellent Tracking, PID, Vertex Performance.
- Belle II aims to collect about  $8 \times 10^{10}$  B mesons by about 2025, roughly 50 more than Belle did
- **Improvement:**
  - New, extended vertex detector 2 pixel layers: DEPFET technology 4 layers of double sided Si microstrip sensors.
  - Smaller cell size and longer lever arm in CDC.
  - Improved electronic and light yield for EM calorimeter.
  - New PID detector for K/  $\pi$  separation
  - Better  $K_s^0$  reconstruction
  - Improved KLM electronics.

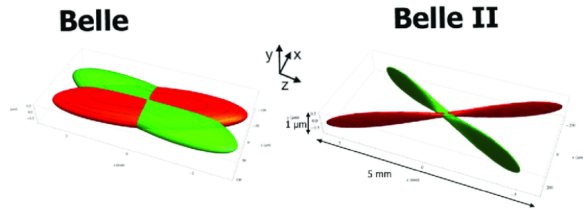


Figure 6: Nano Beam Scheme



Figure 7: Geographical Location of Belle II Detector

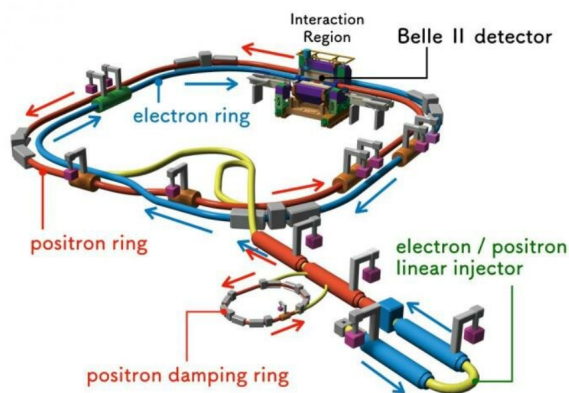


Figure 8: SuperKEKB accelerator (left) and Belle II detector (right).

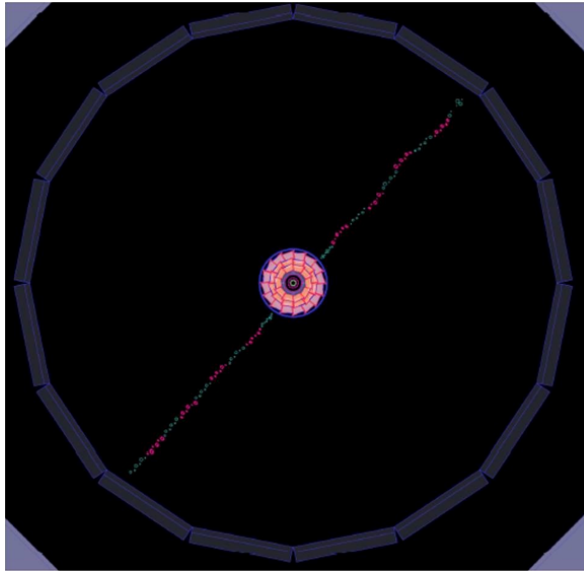


Figure 9: A cosmic muon as recorded by the Belle II Central Drift Chamber (CDC).

- **Vertex Detector:** The new vertex detector is comprised of two devices, the silicon Pixel Detector (PXD) and Silicon Vertex Detector (SVD), with altogether six layers around a 10 mm radius Be beam pipe. The first layers at  $r = 14$  mm and  $r = 22$  mm will use pixelated sensors of the DEPFET type. The remaining four layers at radii of 38 mm, 80 mm, 115 mm, and 140 mm will be equipped with double-sided silicon strip sensors. Compared to the Belle vertex detector, the beam pipe and the first two detector layers are closer to the interaction point, and the outermost layer is at a considerably larger radius. As a result, significant improvement is expected with respect to Belle in the vertex resolution, as well as in the reconstruction efficiency for  $K_s^0 \rightarrow \Pi^+\Pi^-$  decays with hits in the vertex detector.
- **Central Drift Chamber (CDC):** One of the core instruments of the Belle II spectrometer is the central tracking device, a large volume drift chamber with small drift cells. Compared to Belle, it extends to a larger radius (1130 mm compared to 880 mm) due to the upgrade to a much thinner PID device in the barrel region. In total, the CDC contains 14 336 sense wires arranged in 56 layers, either in axial orientation (aligned with the solenoidal magnetic field) or "stereo". By combining information from axial and stereo layers it is possible to reconstruct a full 3D helix track. The chamber gas is comprised of a He-C<sub>2</sub>H<sub>6</sub> 50:50 mixture with an average drift velocity of 3.3 cm/ s and a maximum drift time of about

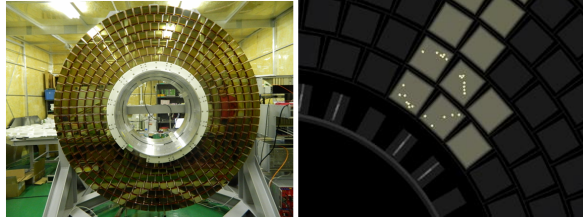


Figure 10: ARICH detector: photon detector plane with HAPD sensors (left); a ring produced by a cosmic muon (right).

350 ns for 17 mm cell size.

- **Particle identification system (TOP and ARICH):** For particle identification in the barrel region, a time-of-propagation (TOP) counter is used. This is a special kind of Cherenkov detector where the two dimensional information of a Cherenkov ring image is given by the time of arrival and impact position of Cherenkov photons at the photo-detector at one end of a 26 m long quartz bar. Each detector module (16 in total) consists of a 45 cm wide and 2 cm thick quartz bar with a small expansion volume (about 10 cm long) at the sensor end of the bar. The expansion wedge introduces some additional pinhole imaging, relaxes slightly the precision timing requirements and reduces the hit occupancy at the photo-detector. The TOP counter requires photo-sensors with a single photon time resolution of about 100 ps, which can be achieved with a 16-channel MCP PMT specially developed for this purpose. In the forward end-cap region, ARICH, a proximity focusing Cherenkov ring imaging detector with aerogel as Cherenkov radiator will be employed to identify charged particles. The design requirements include a low momentum threshold for pions and good separation of pions and kaons from 0.4 GeV/c up to about 4 GeV/c.
- **Electromagnetic Calorimeter (ECL):** The electromagnetic calorimeter is used to detect gamma rays as well as to identify electrons, i.e. separate electrons from hadrons, in particular pions. It is a highly-segmented array of thallium-doped caesium iodide CsI(Tl) crystals assembled in a projective geometry. In the Belle experiment, the energy resolution observed with the same calorimeter was  $\sigma_E/E = 4(3)$  mrad at low (high) energies; 0 mass resolution was  $4.5 \text{ MeV}/c^2$  [2]; in absence of backgrounds a very similar performance would also be expected in Belle II.

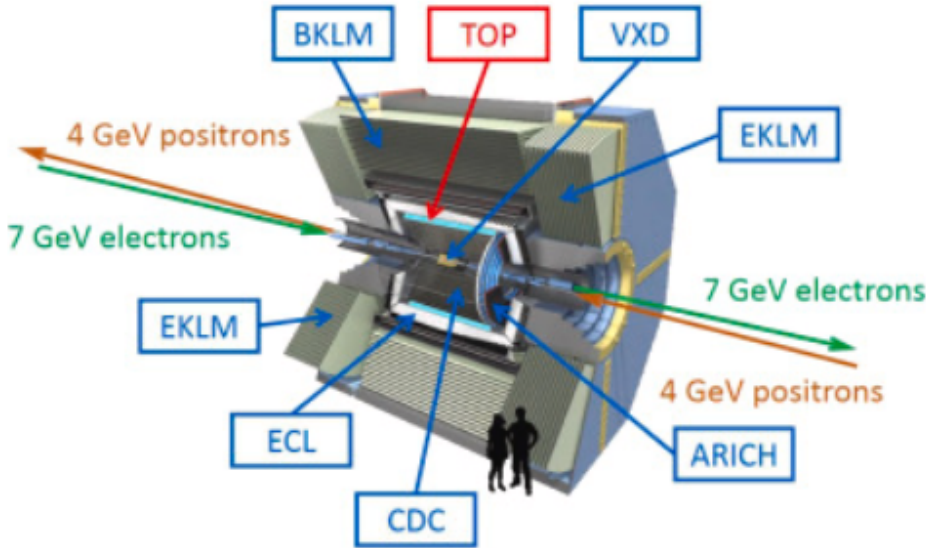


Figure 11: Belle II Detector

- **$K_L$ - Muon Detector (KLM):** The  $K_L^0$  and muon detector (KLM) consists of an alternating sandwich of 4.7 cm thick iron plates and active detector elements located outside the superconducting solenoid. The iron plates serve as the magnetic flux return for the solenoid. They also provide 3.9 interaction lengths or more of material, beyond the 0.8 interaction lengths of the calorimeter, in which  $K_L^0$  mesons can shower hadronically.
- **Trigger System:** The trigger system of Belle II has a non trivial role to identify events of interest during data taking. The scope of physics analysis topics that require dedicated triggers will be broad at Belle II. The agship measurements for Belle II in B- and D- flavour physics are expected to be highly robust to trigger implementation, where events will be easily identified from the presence of at least 3 tracks in the CDC trigger and a large deposition of energy in the ECL. Similarly to Belle, the trigger for most B-decays will be close to 100 that are reconstructed by off fine algorithms.

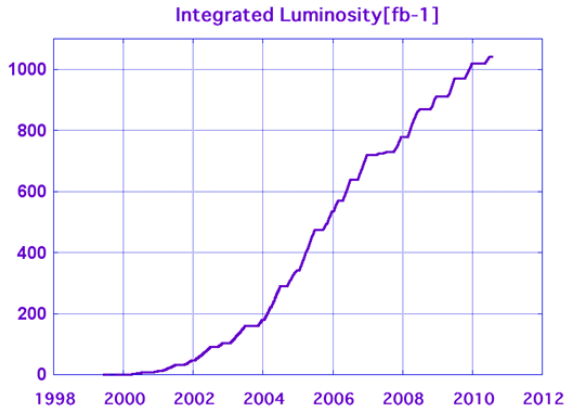


Figure 12: Evolution of Interated Luminosity with Time.

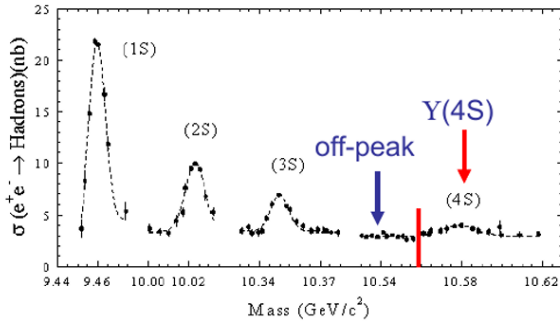


Figure 13:  $e^+e^- \rightarrow \Upsilon(4s) \rightarrow B\bar{B}$

- **Sources of B Hadrons:** CP violating effects are small. Need large number of B mesons to study decay rates with high accuracy.
- B and  $\bar{B}$  come from  $\Upsilon(4s)$  in a coherent  $L = 1$  state.
- $\Upsilon(4s)$  decays strongly so B and  $\bar{B}$  produced as flavor eigenstates. After production, each meson oscillates in time, but in phase so that at any time there is only one B and one  $\bar{B}$  until one particle decays. Once one B decays, the other continues to oscillate, but coherence is broken. Possible to have events with two B or two  $\bar{B}$  decays.
- This common evolution will become important for CP studies. Time integrate asymmetries vanish for cases where CP violation comes from mixing diagrams.

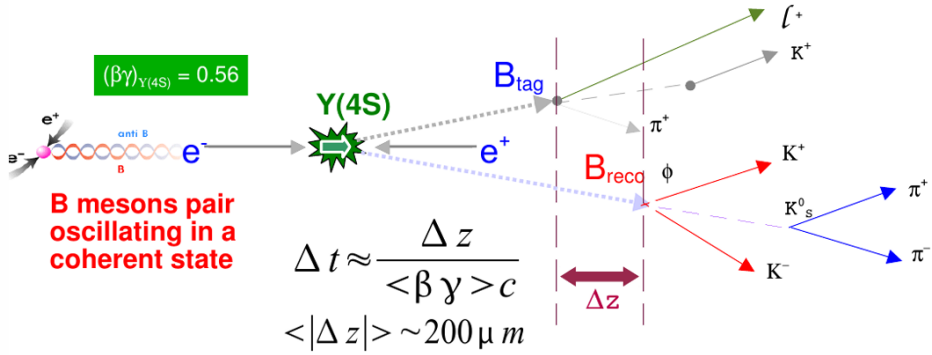


Figure 14: Production of  $B\bar{B}$ .

- In addition, in center-of-mass,  $B$  hadrons have almost no momentum. Difficult to distinguish which tracks come from  $B$  and which from  $\bar{B}$ .
- Initially we have  $e^+$  and  $e^-$  beams with different energies. After the production  $\Upsilon(4s)$  is boosted along beamline.  $B$  mesons travel finite distance before decaying. Typical distance between decay of the two  $B$  mesons  $\sim 200 \mu m$ .

## 9.4 LHCb Experiment

$pp$  or  $p\bar{p} \rightarrow b\bar{b} + X$

- The LHCb detector is a forward spectrometer, and is installed at Intersection Point 8 of the LHC.
- Its primary aim is to investigate the decays of  $B$ -particles (particles containing  $b$ -quarks) and so provide insight into the phenomenon of matter-antimatter asymmetries.
- This results in a detector length of approximately 20 m, and with maximum transverse dimensions about 65 m<sup>3</sup>. The angular acceptance ranges from approximately 10 mrad to 300 mrad.
- LHCb started taking data in 2010.

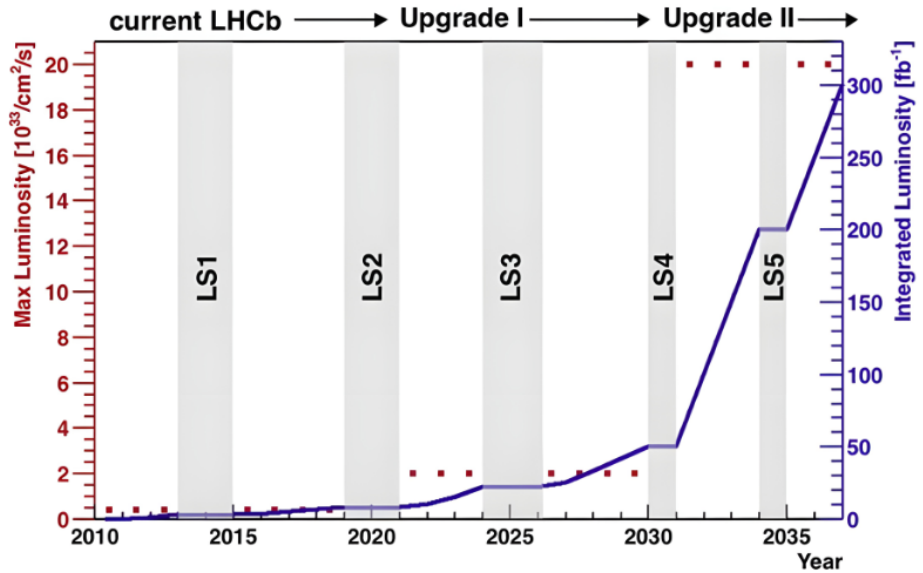


Figure 15: Evolution of Maximum Luminosity of LHCb with Time.

- The Run 1 commenced at an initial centre of mass energy of  $s = 7 \text{ TeV}$  which was then increased to  $s = 8 \text{ TeV}$ , collecting an integrated luminosity of  $323 \text{ fb}^{-1}$  until the end of 2012.
- LHC operation continued from 2015 to 2018 (Run 2), when the experiment took data at  $s = 13 \text{ TeV}$ , recording an integrated luminosity of  $6 \text{ fb}^{-1}$ .
- The collaboration comprises almost 1000 physicists and engineers from more than 65 institutes from all over the world.

## 10 Experimental Results

### TD CPV Measurement:

- $B^0 \rightarrow J/\psi K_s^0$   
SM gives  $A=0$   $B=\sin 2\beta$ . Experimentally very clean determination of !  $S_f = \sin 2\beta = 0.667 \pm 0.023 \pm 0.012$   $A_f = 0.006 \pm 0.016 \pm 0.012$ .
- $B^0 \rightarrow \eta' K^0$   $S_{\eta' K^0} = 0.68 \pm 0.07(\text{stat}) \pm 0.03(\text{syst})$   
 $A_{\eta' K^0} = 0.03 \pm 0.05(\text{stat}) \pm 0.07(\text{syst})$

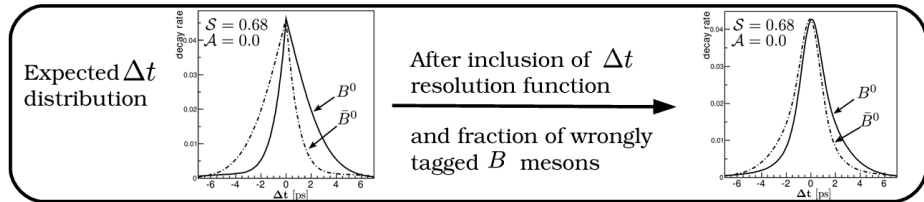


Figure 16: Distribution of  $\Delta t$

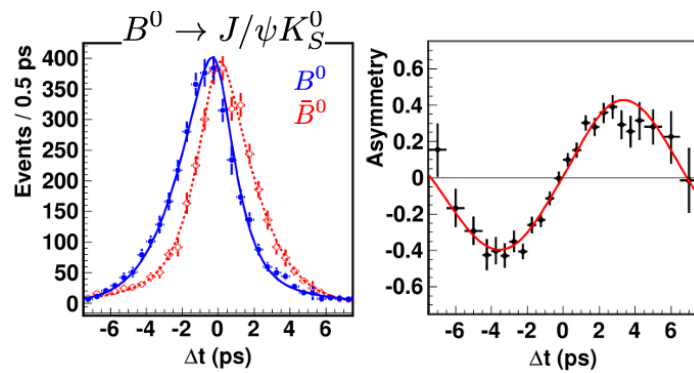


Figure 17: Event Distribution(Left), Asymmetry (Right) with  $\Delta t$

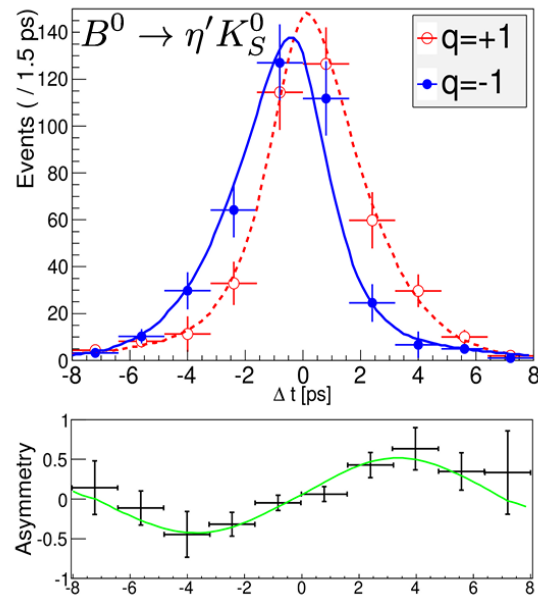


Figure 18: Event Distribution(Left), Asymmetry (Right) with  $\Delta t$

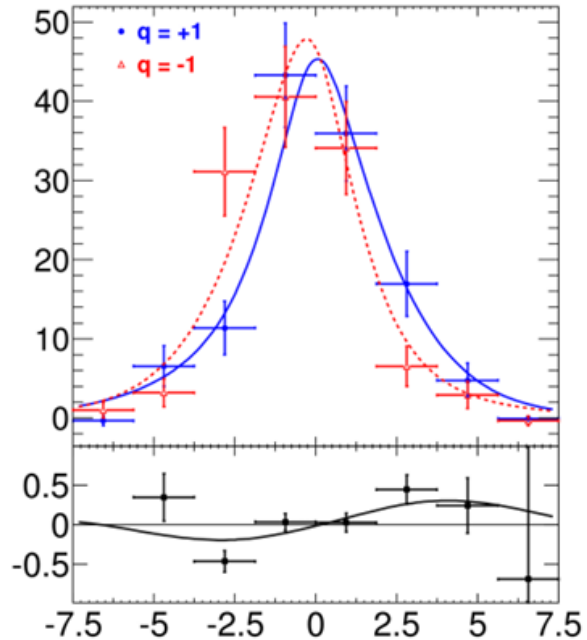


Figure 19: Event Distribution(Top), Asymmetry (Bottom) with  $\Delta t$

- $B^0 \rightarrow \omega K_s^0$   $S_{\omega K_s^0} = 0.91 \pm 0.31(stat) \pm 0.05(syst)$   
 $A_{\omega K_s^0} = -0.36 \pm 0.19(stat) \pm 0.05(syst)$

## 11 Determination of $|V_{ub}|$

The magnitude of the CKM matrix element  $|V_{ub}|$  plays a crucial role in testing the Standard Model description of flavor and CP violation. Its determination is challenging due to the smallness of  $|V_{ub}|$  relative to other CKM elements, and two primary methods have been developed:

1. **Exclusive Determinations:** Involve the analysis of specific decay channels such as  $B \rightarrow \pi \ell \nu$ ,  $B \rightarrow \rho \ell \nu$ , and others.
2. **Inclusive Determinations:** Involve summing over all possible charmless semileptonic decays, i.e.  $B \rightarrow X_u \ell \nu$ , where  $X_u$  represents any hadronic state resulting from a  $b \rightarrow u$  transition.

Both approaches have unique advantages and theoretical challenges.

### 11.1 Exclusive Determination: $B \rightarrow \pi \ell \nu$

The exclusive decay  $B \rightarrow \pi \ell \nu$  proceeds via a tree-level  $b \rightarrow u$  transition mediated by a  $W$  boson. The effective Hamiltonian for this process is given by

$$\mathcal{H}_{\text{eff}} = \frac{G_F}{\sqrt{2}} V_{ub} \bar{u} \gamma^\mu (1 - \gamma^5) b \bar{\ell} \gamma_\mu (1 - \gamma^5) \nu_\ell. \quad (45)$$

**Hadronic Matrix Element:** The central nonperturbative object is the hadronic matrix element

$$\langle \pi(p_\pi) | \bar{u} \gamma^\mu b | B(p_B) \rangle, \quad (46)$$

which is parameterized in terms of form factors. Since the pion is a pseudoscalar, the vector current matrix element is written as

$$\langle \pi(p_\pi) | \bar{u} \gamma^\mu b | B(p_B) \rangle = f_+(q^2) \left[ (p_B + p_\pi)^\mu - \frac{m_B^2 - m_\pi^2}{q^2} q^\mu \right] + f_0(q^2) \frac{m_B^2 - m_\pi^2}{q^2} q^\mu, \quad (47)$$

with

$$q^\mu = p_B^\mu - p_\pi^\mu, \quad q^2 \in [0, (m_B - m_\pi)^2].$$

In practice, only  $f_+(q^2)$  contributes because the lepton mass is negligible (except for the tau mode).

**Differential Decay Rate:** The double differential decay rate in the  $B$  rest frame is derived by squaring the amplitude. Neglecting the lepton masses, one obtains

$$\frac{d\Gamma(B \rightarrow \pi \ell \nu)}{dq^2} = \frac{G_F^2 |V_{ub}|^2}{192\pi^3 m_B^3} \lambda^{3/2}(q^2) |f_+(q^2)|^2, \quad (48)$$

where  $\lambda(q^2)$  is the standard triangle function:

$$\lambda(q^2) = \left[ (m_B + m_\pi)^2 - q^2 \right] \left[ (m_B - m_\pi)^2 - q^2 \right]. \quad (49)$$

A derivation of Eq. (48) proceeds by writing the invariant amplitude  $\mathcal{M}$  as

$$\mathcal{M} = \frac{G_F}{\sqrt{2}} V_{ub} \langle \pi(p_\pi) | \bar{u} \gamma^\mu b | B(p_B) \rangle L_\mu,$$

with the leptonic current

$$L_\mu = \bar{\ell}(p_\ell) \gamma_\mu (1 - \gamma^5) \nu_\ell(p_\nu).$$

Squaring the matrix element, summing (averaging) over final (initial) spin states, and integrating over the three-body phase space yields Eq. (48).

**Extraction of  $|V_{ub}|$ :** By measuring the differential decay rate  $d\Gamma/dq^2$  experimentally and combining it with theoretical computations of  $f_+(q^2)$  (from lattice QCD at high  $q^2$  and light-cone sum rules at low  $q^2$ ), one extracts  $|V_{ub}|$ .

### Drawbacks and Uncertainties:

- **Form Factor Uncertainties:** The theoretical determination of  $f_+(q^2)$  is subject to systematic uncertainties. While lattice QCD is precise at high  $q^2$ , matching with sum-rule results at low  $q^2$  introduces model dependence.
- **Limited Phase Space:** Experimental measurements may only cover part of the  $q^2$  range, requiring extrapolations.
- **Parametrization Dependencies:** Different parameterizations of  $f_+(q^2)$  (e.g., Boyd-Grinstein-Lebed or Bourrely-Caprini-Lellouch) can lead to variations in the extracted value.

## 11.2 Inclusive Determination: $B \rightarrow X_u \ell \nu$

Unlike the exclusive method, the inclusive approach considers the total rate for all charmless semileptonic decays  $B \rightarrow X_u \ell \nu$ . The theoretical framework is based on the heavy-quark expansion (HQE) and the operator product expansion (OPE).

**Effective Theory and Optical Theorem:** The total decay rate is computed using the optical theorem. In the heavy-quark limit, one writes

$$\Gamma(B \rightarrow X_u \ell \nu) = \frac{1}{2m_B} \langle B | \text{Im } T | B \rangle, \quad (50)$$

where the transition operator  $T$  is defined as

$$T = i \int d^4x T \left\{ \mathcal{H}_{\text{eff}}(x) \mathcal{H}_{\text{eff}}(0) \right\}. \quad (51)$$

For  $b \rightarrow u$  transitions the effective Hamiltonian is given in Eq. (45).

**Leading Order Expression:** At leading order in the HQE, the total decay rate is

$$\Gamma(B \rightarrow X_u \ell \nu) = \frac{G_F^2 |V_{ub}|^2 m_b^5}{192\pi^3} \left[ 1 + \mathcal{O}(\alpha_s) + \mathcal{O}(1/m_b^2) \right]. \quad (52)$$

Here,  $m_b$  is the  $b$ -quark mass. Radiative corrections (in  $\alpha_s$ ) and nonperturbative corrections (in powers of  $1/m_b^2$ ) can be systematically included.

**Kinematic Cuts and Shape Functions:** A major experimental challenge is that the dominant semileptonic decay channel  $B \rightarrow X_c \ell \nu$  is about 50 times larger than  $B \rightarrow X_u \ell \nu$ . To reduce the background, experiments apply kinematic cuts—for example, on the lepton energy  $E_\ell$  or on the invariant mass of the hadronic final state  $m_X$ . Near the endpoint of the lepton energy spectrum, the OPE breaks down and one must resum an infinite series of leading-twist contributions. This resummation is encoded in a nonperturbative *shape function*  $f(k_+)$  (with  $k_+$  a light-cone component of the residual momentum), which modifies the differential decay rates. For example, the differential rate can be written schematically as

$$\frac{d\Gamma}{dE_\ell} \sim \int dk_+ f(k_+) \left( \frac{d\hat{\Gamma}}{dE_\ell} \right) (m_b^* = m_b + k_+), \quad (53)$$

where  $\frac{d\hat{\Gamma}}{dE_\ell}$  is the partonic decay rate evaluated with an effective heavy-quark mass  $m_b^*$ .

## Drawbacks and Uncertainties:

- **Background Suppression:** Kinematic cuts designed to suppress  $b \rightarrow c$  decays also enhance sensitivity to the poorly known endpoint region.
- **Shape Function Model Dependence:** The extraction of  $|V_{ub}|$  depends on the model used for the shape function and its corresponding uncertainties.
- **Higher-Order Corrections:** Radiative corrections and higher-order power corrections must be carefully estimated.

### 11.3 Comparison and Numerical Extraction of $|V_{ub}|$

**Exclusive vs. Inclusive:** While exclusive decays rely on detailed knowledge of form factors—calculated by lattice QCD and sum rules—the inclusive method benefits from the universality of the heavy-quark expansion. However, the need for tight kinematic cuts in the inclusive analysis introduces its own set of uncertainties, particularly related to the modeling of the shape function.

**Numerical Results:** In practice, analyses typically find:

- **Exclusive Methods:** Values of

$$|V_{ub}|_{\text{excl}} \approx (3.82 \pm 0.20) \times 10^{-3},$$

where the dominant uncertainties arise from the determination of the form factor  $f_+(q^2)$ .

- **Inclusive Methods:** Values of

$$|V_{ub}|_{\text{incl}} \approx (4.13 \pm 0.12^{+0.13}_{-0.14} \pm 0.18) \times 10^{-3},$$

where the first error is experimental, the second arises from the model dependence quoted by the individual measurements, and the third is an additional one estimated in Grinstein, 2017

The tension between these two values remains an active topic of research, with improvements in both theoretical inputs and experimental techniques continually sought.

## 12 Conclusion

The Standard Model’s description of CP violation through the CKM matrix remains remarkably consistent across decades of precision tests. From first principles—electroweak symmetry breaking and Yukawa interactions—to the  $> 5\sigma$  observational evidence for CP asymmetry in  $B$ -meson systems, the CKM paradigm successfully encodes flavor violation within a single Jarlskog invariant  $J = (3.0 \pm 0.2) \times 10^{-5}$ . Key achievements include:

- Determination of CKM angles to sub-degree precision:  $\beta = (21.85 \pm 0.28)^\circ$ ,  $\gamma = (65.4 \pm 1.1)^\circ$ ;
- Validation of CKM unitarity via  $\Delta m_{d,s}$  measurements ( $|V_{td}/V_{ts}| = 0.210 \pm 0.004$ );
- Exclusion of minimal SUSY and other NP models as dominant CP sources at  $\mathcal{O}(10^{-3})$  precision.

Persistent tensions, however, signal unresolved challenges. The  $2.5\sigma$  discrepancy between inclusive ( $|V_{ub}| = 4.13(25) \times 10^{-3}$ ) and exclusive ( $|V_{ub}| = 3.82(20) \times 10^{-3}$ ) determinations underscores limitations in heavy-quark expansions and lattice QCD form factors. Similarly, the  $3.1\sigma$  anomaly in  $B^+ \rightarrow K^+ \ell^+ \ell^-$  angular distributions **LHCb2023** hints at potential lepton universality violations orthogonal to CKM dynamics.

Upgraded experiments—Belle II ( $50 \text{ ab}^{-1}$ ), LHCb Run 3 ( $300 \text{ fb}^{-1}$ ), and the proposed FCC-ee—will probe CKM parameters at the 0.1% level while searching for  $CP$  violation beyond quark mixing. Concurrent advances in lattice QCD (sub-1%  $f_+^{B\pi}$  precision) and non-perturbative shape functions will sharpen SM predictions.

Ultimately, the CKM matrix’s economy in explaining  $CP$  violation remains both its strength and limitation. While no definitive beyond-SM signatures have emerged, the path forward lies in exploiting tensions between theory and experiment—whether resolving them within the SM or exposing its incompleteness. Either outcome will deepen our understanding of nature’s fundamental asymmetries.

## References

- Aggarwal, L., Banerjee, S., Bansal, S., Bernlochner, F., Bertemes, M., Bhardwaj, V., Bondar, A., Browder, T. E., Cao, L., Campajola, M., Casarosa, G., Cecchi, C., Cheaib, R., Pietro, G. D., Canto, A. D., Dorigo, M., Feichtinger, P., Ferber, T., Fulsom, B., García, M., Gaudino, G., Gaz, A., Glazov, A., Granderath, S., Graziani, E., Greenwald, D., Goldenzweig, P., Heredia, I., Villanueva, M. H., Higuchi, T., Humair, T., Iijima, T., Inguglia, G., Ishikawa, A., Jacobi, D., Junkerkalefeld, H. A., Karl, R., Lautenbach, K., Lewis, P. M., Li, L.-K., La-prapara, S., Libby, J., Manoni, E., Martini, A., Merola, M., Milesi, M., Moneta, S., Nayak, M., Nishida, S., Palaia, M. A., Pham, F., Polat, L., Prell, S. A., Prencipe, E., Räuber, G., Ripp-Baudot, I., Rhorken, M., Roney, M., Rostomyan, A., Sakai, Y., Sato, Y., Schwanda, C., Schwartz, A. J., Serrano, J., Sutcliffe, W., Svidras, H., Tackmann, K., Tamponi, U., Tenchini, F., Trabelsi, K., Tiwary, R., Tonelli, D., Uno, K., Vossen, A., Yabsley, B., Yin, J.-H., & Zani, L. (2022). Snowmass white paper: Belle ii physics reach and plans for the next decade and beyond.
- Beringer, J., Arguin, J. .-, Barnett, R. M., Copic, K., Dahl, O., Groom, D. E., Lin, C. .-, Lys, J., Murayama, H., Wohl, C. G., Yao, W. .-, Zyla, P. A., Amsler, C., Antonelli, M., Asner, D. M., Baer, H., Band, H. R., Basaglia, T., Bauer, C. W., Beatty, J. J., Belousov, V. I., Bergren, E., Bernardi, G., Bertl, W., Bethke, S., Bichsel, H., Biebel, O., Blucher, E., Blusk, S., Brooijmans, G., Buchmueller, O., Cahn, R. N., Carena, M., Ceccucci, A., Chakraborty, D., Chen, M. .-, Chivukula, R. S., Cowan, G., D'Ambrosio, G., Damour, T., de Florian, D., de Gouvêa, A., DeGrand, T., de Jong, P., Dissertori, G., Dobrescu, B., Doser, M., Dreess, M., Edwards, D. A., Eidelman, S., Erler, J., Ezhela, V. V., Fettscher, W., Fields, B. D., Foster, B., Gaisser, T. K., Garren, L., Gerber, H. .-, Gerbier, G., Gherghetta, T., Golwala, S., Goodman, M., Grab, C., Gritsan, A. V., Grivaz, J. .-, Grünewald, M., Gurtu, A., Gutsche, T., Haber, H. E., Hagiwara, K., Hagmann, C., Hanhart, C., Hashimoto, S., Hayes, K. G., Heffner, M., Heltsley, B., Hernández-Rey, J. J., Hikasa, K., Höcker, A., Holder, J., Holtkamp, A., Huston, J., Jackson, J. D., Johnson, K. F., Junk, T., Karlen, D., Kirkby, D., Klein, S. R., Klempert, E., Kowalewski, R. V., Krauss, F., Kreps, M., Krusche, B., Kuyanov, Y. V., Kwon, Y., Lahav, O., Laiho, J., Langacker, P., Liddle, A., Ligeti, Z., Liss, T. M., Littenberg, L., Lugovsky, K. S., Lugovsky, S. B., Mannel, T., Manohar, A. V., Marciano, W. J., Martin, A. D., Masoni, A., Matthews, J.,

Milstead, D., Miquel, R., Mönig, K., Moortgat, F., Nakamura, K., Narain, M., Nason, P., Navas, S., Neubert, M., Nevski, P., Nir, Y., Olive, K. A., Pape, L., Parsons, J., Patrignani, C., Peacock, J. A., Petcov, S. T., Piepke, A., Pomarol, A., Punzi, G., Quadrt, A., Raby, S., Raffelt, G., Ratcliff, B. N., Richardson, P., Roesler, S., Rolli, S., Romaniouk, A., Rosenberg, L. J., Rosner, J. L., Sachrajda, C. T., Sakai, Y., Salam, G. P., Sarkar, S., Sauli, F., Schneider, O., Scholberg, K., Scott, D., Seligman, W. G., Shaevitz, M. H., Sharpe, S. R., Silari, M., Sjöstrand, T., Skands, P., Smith, J. G., Smoot, G. F., Spanier, S., Spieler, H., Stahl, A., Staney, T., Stone, S. L., Sumiyoshi, T., Syphers, M. J., Takahashi, F., Tanabashi, M., Terning, J., Titov, M., Tkachenko, N. P., Törnqvist, N. A., Tovey, D., Valencia, G., van Bibber, K., Venanzoni, G., Vincter, M. G., Vogel, P., Vogt, A., Walkowiak, W., Walter, C. W., Ward, D. R., Watari, T., Weiglein, G., Weinberg, E. J., Wiencke, L. R., Wolfenstein, L., Womersley, J., Woody, C. L., Workman, R. L., Yamamoto, A., Zeller, G. P., Zenin, O. V., Zhang, J., Zhu, R. .-, Harper, G., Lugovsky, V. S., & Schaffner, P. (2012). Review of particle physics. *Phys. Rev. D*, *86*, 010001. <https://doi.org/10.1103/PhysRevD.86.010001>

Collaboration, B. I., Adachi, I., Aggarwal, L., Ahmed, H., Aihara, H., Akopov, N., Aloisio, A., Ky, N. A., Asner, D. M., Atmacan, H., Aushev, T., Aushev, V., Aversano, M., Babu, V., Bae, H., Bahinipati, S., Bambade, P., Banerjee, S., Barrett, M., Baudot, J., Baur, A., Beaubien, A., Becherer, F., Becker, J., Bennett, J. V., Bernlochner, F. U., Bertacchi, V., Bertemes, M., Bertholet, E., Bessner, M., Bettarini, S., Bhuyan, B., Bianchi, F., Bilka, T., Bilokin, S., Biswas, D., Bobrov, A., Bodrov, D., Bolz, A., Bondar, A., Borah, J., Bozek, A., Bračko, M., Branchini, P., Briere, R. A., Browder, T. E., Budano, A., Bussino, S., Campajola, M., Cao, L., Casarosa, G., Cecchi, C., Cerasoli, J., Chang, M. .-, Chang, P., Cheema, P., Chen, C., Cheon, B. G., Chilikin, K., Chirapatpimol, K., Cho, H. .-, Cho, K., Cho, S. .-, Choi, S. .-, Choudhury, S., Corona, L., Das, S., Dat-tola, F., Cruz-Burelo, E. D. L., Motte, S. A. D. L., Nardo, G. D., Nuccio, M. D., Pietro, G. D., de Sangro, R., Destefanis, M., Dhamija, R., Canto, A. D., Capua, F. D., Dingfelder, J., Doležal, Z., Dong, T. V., Dorigo, M., Dort, K., Dreyer, S., Dubey, S., Dujany, G., Ecker, P., Eliachevitch, M., Feichtinger, P., Ferber, T., Ferlewicz, D., Fillinger, T., Finck, C., Finocchiaro, G., Fodor, A., Forti, F., Frey, A., Fulsom, B. G., Gabrielli, A., Ganiev, E., Garcia-Hernandez, M., Garg, R., Gaudino, G., Gaur, V., Gaz, A., Gellrich, A., Ghevondyan, G., Ghosh, D., Ghu-

maryan, H., Giakoustidis, G., Giordano, R., Giri, A., Gobbo, B., Godang, R., Gogota, O., Goldenzweig, P., Gradl, W., Grammatico, T., Graziani, E., Greenwald, D., Gruberová, Z., Gu, T., Guan, Y., Gudkova, K., Halder, S., Han, Y., Hara, K., Hara, T., Hayashii, H., Hazra, S., Hearty, C., Hedges, M. T., Heidelbach, A., de la Cruz, I. H., Villanueva, M. H., Higuchi, T., Hoek, M., Hohmann, M., Horak, P., Hsu, C. . ., Humair, T., Iijima, T., Ipsita, N., Ishikawa, A., Itoh, R., Iwasaki, M., Jackson, P., Jacobs, W. W., Jang, E. . ., Ji, Q. P., Jia, S., Jin, Y., Joo, K. K., Junkerkalefeld, H., Kakuno, H., Kalita, D., Kaliyar, A. B., Kandra, J., Kang, K. H., Kang, S., Karyan, G., Kawasaki, T., Keil, F., Kiesling, C., Kim, C. . ., Kim, D. Y., Kim, K. . ., Kim, Y. . ., Kindo, H., Kinoshita, K., Kodyš, P., Koga, T., Kohani, S., Kojima, K., Korobov, A., Korpar, S., Kovalenko, E., Kowalewski, R., Kraetzschnmar, T. M. G., Križan, P., Krokovny, P., Kuhr, T., Kulii, Y., Kumar, J., Kumar, M., Kumara, K., Kunigo, T., Kuzmin, A., Kwon, Y. . ., Lacaprara, S., Lai, Y. . ., Lam, T., Lanceri, L., Lange, J. S., Laurenza, M., Leboucher, R., Diberder, F. R. L., Lee, M. J., Levit, D., Li, C., Li, L. K., Li, Y., Li, Y. B., Libby, J., Liu, M., Liu, Q. Y., Liu, Z. Q., Liventsev, D., Longo, S., Lueck, T., Lyu, C., Ma, Y., Maggiora, M., Maharana, S. P., Maiti, R., Maity, S., Mancinelli, G., Manfredi, R., Manoni, E., Mantovano, M., Marcantonio, D., Marcello, S., Marinas, C., Martel, L., Martellini, C., Martini, A., Martinov, T., Massaccesi, L., Masuda, M., Matsuoka, K., Matvienko, D., Maurya, S. K., McKenna, J. A., Mehta, R., Meier, F., Merola, M., Metzner, F., Miller, C., Mirra, M., Miyabayashi, K., Miyake, H., Mizuk, R., Mohanty, G. B., Molina-Gonzalez, N., Mondal, S., Moneta, S., Moser, H. . ., Mrvar, M., Mussa, R., Nakamura, I., Nakazawa, Y., Charan, A. N., Naruki, M., Narwal, D., Natkaniec, Z., Natochii, A., Nayak, L., Nayak, M., Nazaryan, G., Niebuhr, C., Nishida, S., Ogawa, S., Onishchuk, Y., Ono, H., Onuki, Y., Oskin, P., Otani, F., Pakhlov, P., Pakhlova, G., Panta, A., Pardi, S., Parham, K., Park, H., Park, S. . ., Paschen, B., Passeri, A., Patra, S., Paul, S., Pedlar, T. K., Peschke, R., Pestotnik, R., Piccolo, M., Piilonen, L. E., Podesta-Lerma, P. L. M., Podobnik, T., Pokharel, S., Praz, C., Prell, S., Prencipe, E., Prim, M. T., Purwar, H., Rados, P., Raeuber, G., Raiz, S., Rauls, N., Reif, M., Reiter, S., Remnev, M., Ripp-Baudot, I., Rizzo, G., Robertson, S. H., Roehrken, M., Roney, J. M., Rostomyan, A., Rout, N., Russo, G., Sanders, D. A., Sandilya, S., Santelj, L., Sato, Y., Savinov, V., Scavino, B., Schmitt, C., Schwanda, C., Schwartz, A. J., Seino, Y., Selce, A., Senyo, K., Serrano, J., Sevior, M. E., Sfienti, C., Shan, W., Shi, X. D., Shilling-

- ton, T., Shimasaki, T., Shiu, J. ., Shtol, D., Sibidanov, A., Simon, F., Singh, J. B., Skorupa, J., Sobie, R. J., Sobotzik, M., Soffer, A., Sokolov, A., Solovieva, E., Spataro, S., Spruck, B., Starić, M., Stavroulakis, P., Stefkova, S., Stroili, R., Sumihama, M., Sumisawa, K., Sutcliffe, W., Svidras, H., Takizawa, M., Tamponi, U., Tanaka, S., Tanida, K., Tenchini, F., Tittel, O., Tiwary, R., Tonelli, D., Torassa, E., Trabelsi, K., Tsaklidis, I., Uchida, M., Ueda, I., Uematsu, Y., Uglov, T., Unger, K., Unno, Y., Uno, K., Uno, S., Urquijo, P., Ushiroda, Y., Vahsen, S. E., van Tonder, R., Varvell, K. E., Veronesi, M., Vinokurova, A., Vismaya, V. S., Vitale, L., Vobbillisetti, V., Volpe, R., Wach, B., Wakai, M., Wallner, S., Wang, E., Wang, M. ., Wang, X. L., Wang, Z., Warburton, A., Watanuki, S., Wessel, C., Won, E., Xu, X. P., Yabsley, B. D., Yamada, S., Yang, S. B., Yelton, J., Yin, J. H., Yoshihara, K., Yuan, C. Z., Yusa, Y., Zhang, B., Zhang, Y., Zhilich, V., Zhou, Q. D., Zhou, X. Y., & Zhukova, V. I. (2024). Measurement of  $CP$  asymmetries in  $B^0 \rightarrow K_s^0$  decays at belle ii. *Phys. Rev. D* 110, 112002, Published 2 December, 2024. <https://doi.org/10.1103/PhysRevD.110.112002>
- Fleischer, R. (2024). CP violation in B decays: recent developments and future perspectives. *Eur. Phys. J. ST*, 233(2), 391–408. <https://doi.org/10.1140/epjs/s11734-024-01127-0>
- Grinstein, B. (2017). Determination of vub and vcb from semileptonic decays, 061. <https://doi.org/10.22323/1.274.0061>
- Grossman, Y., & Nir, Y. (2023, September). *The standard model: From fundamental symmetries to experimental tests* [NA]. Princeton University Press.
- Jarlskog, C. (1985). Commutator of the quark mass matrices in the standard electroweak model and a measure of maximal cp violation [Defines the Jarlskog invariant as a measure of CP violation]. *Phys. Rev. Lett.*, 55, 1039–1042. <https://doi.org/10.1103/PhysRevLett.55.1039>
- Licata, C. L. (2018). Belle ii prospects for cp-violation measurements. <https://doi.org/10.5506/APhysPolB.49.1229>
- Mandal, R., Ananthanarayan, B., & Wyler, D. (2024). b-Quark physics as a precision laboratory: a collection of articles on the present status and future prospects. *The European Physical Journal Special Topics*, 233(2), 209–211. <https://doi.org/10.1140/epjs/s11734-024-01163-w>
- Schwartz, M. D. (2014, March). *Quantum Field Theory and the Standard Model*. Cambridge University Press.

Wolfenstein, L. (1983). Parametrization of the kobayashi-maskawa matrix [Introduces the Wolfenstein parameterization for the CKM matrix]. *Phys. Rev. Lett.*, 51, 1945–1947. <https://doi.org/10.1103/PhysRevLett.51.1945>